Journal of Power Sources 196 (2011) 1608–1614

Contents lists available at ScienceDirect

Journal of Power Sources

journal homepage: www.elsevier.com/locate/jpowsour

Syntheses of polyaniline/ordered mesoporous carbon composites with interpenetrating framework and their electrochemical capacitive performance in alkaline solution

Yu-Qian Dou [a], Yunpu Zhai [b], Haijing Liu [b], Yongyao Xia [b], Bo Tu [b], Dongyuan Zhao [b], Xiao-Xia Liu [a,*]

[a] Department of Chemistry, Northeastern University, Shenyang 110819, China
[b] Department of Chemistry, Shanghai Key Laboratory of Molecular Catalysis and Innovative Materials, Key Laboratory of Molecular Engineering of Polymers of the Chinese Ministry of Education, Laboratory of Advanced Materials, Fudan University, Shanghai 200433, China

ARTICLE INFO

Article history:
Received 1 June 2010
Received in revised form 3 August 2010
Accepted 2 September 2010
Available online 15 September 2010

Keywords:
Polyaniline
Ordered mesoporous carbon
Interpenetrating framework composites
Negative electrode materials
Supercapacitor

ABSTRACT

Composites of polyaniline (PANI) and a unique ordered mesoporous carbon MPC which possesses small pores inside the carbon walls have been prepared. The monomer (aniline) of PANI is firstly soaked in the small pores inside the carbon walls and then confined in the primary mesochannels as well with increasing the concentration of aniline in the soaking solution. After the following *in situ* polymerization, composites of PANI and MPC with bicontinuous interpenetrating framework are formed. The composites show significant redox activities at potentials negative to 0 V *vs.* Hg/HgO in a strong alkaline solution, which is unusual for PANI and PANI based composites as PANI usually loses its electrochemical activity at pH > 4. The specific capacitance of the composites is as high as 400 F g^{-1} at a high current density of 1 A g^{-1} in the potential range of −0.7 to 0 V, which is twice higher than that of the host MPC. The capacitance only decreases about 9% when the discharge current density increases from 1 to 20 A g^{-1}, indicative of excellent rate capability. Therefore, the composites are very promising for the application as electrode materials in supercapacitors, especially as materials for negative electrode in hybrid supercapacitors.

1. Introduction

Supercapacitors have attracted great interests in energy storage field due to their large power capability, high efficiency and long cycle life [1,2]. However, the energy density (E) of supercapacitors is usually lower than that of batteries. The energy density is proportional to the specific capacitance (C_{sp}) and the square of operating voltage (V) according to the formula:

$$E = 0.5\, C_{sp} V^2 \quad (1)$$

The operating voltage of hybrid supercapacitors, in which the positive and negative electrodes are constructed by different materials, can be broadened as the two electrodes accumulate charge in different potential ranges. So hybrid supercapacitors exhibit great advantages in enhancement of the energy density [3–8]. Most of the hybrid supercapacitors developed to date have adopted pseudocapacitive materials, including manganese oxides [3,4], vanadium oxides [5], nickel oxides [6], and conducting polymers [7,8] as the positive electrode. These electrodes can accumulate charge through faradic electrochemical process (redox reactions), which generate higher capacitance relative to those through electrical double layer. However, pseudocapacitive materials for negative electrode are very limited as few materials show good reversible and stable electrochemical activity in low potential range. The most commonly used negative electrode materials in hybrid supercapacitors are activated carbons as they can store charges in negative potential range. Activated carbons also possess other merits such as non-toxicity, good conductivity and high chemical stability [9–11]. However, as the specific capacitance of carbon materials mainly derives from electrical double-layer capacitance, their specific capacitance is usually much lower than that of the positive electrode. In order to match with the positive electrode, the mass of the negative carbon based electrode should be larger, which will increase the total mass (M) of the supercapacitor. The capacitance (C) of a supercapacitor is a series sum of the capacitance at positive electrode (C_p) and negative electrode (C_n) according to the equation: $1/C = 1/C_p + 1/C_n$, while the total specific capacitance C_{sp} of a supercapacitor is related to the total mass M according to the formula: $C_{sp} = C/M$. Therefore, for the sake of increasing the total specific capacitance of a hybrid supercapacitor, it is meaningful to exploit materials with high specific capacitance in negative potential range. In addition, the ultra micropores and randomly connected pore structure of activated carbons are disadvantageous for the diffusion of solvated ions, especially at high current den-

* Corresponding author. Tel.: +86 24 23600159; fax: +86 24 83689510.
E-mail address: xxliu@mail.neu.edu.cn (X.-X. Liu).

0378-7753/$ – see front matter © 2010 Elsevier B.V. All rights reserved.
doi:10.1016/j.jpowsour.2010.09.005

sity. As a result, high rate capability, which is very important for high power supercapacitors, cannot be realized [12]. In order to get hybrid supercapacitors with desirable properties, considerable effort should be invested in developing better negative electrode materials.

Highly ordered mesoporous carbons (OMCs) have been recognized as good candidates of electrode materials for supercapacitors due to their high surface area, narrow pore size distribution and uniform pore connections [13]. The mesopores and micropores are perfectly interconnected in OMCs, which is more favorable for fast ionic transport than the pore networks in disordered microporous carbons. Therefore, OMCs have showed superior capacitive behavior and better power output performance than conventional activated carbons in supercapacitors [14]. However, the specific capacitance of OMCs is still not quite satisfying as negative electrode materials in hybrid supercapacitors. Great efforts have been made to improve charge storage properties of OMCs. An efficient method to enhance the specific capacitance of OMCs is to incorporate other materials which can provide high pseudocapacitance through redox reactions, such as metal oxides and nitrides [15], conducting polymers [16,17]. Among these candidates, polyaniline (PANI), as a key material in the family of conducting polymers, has been extensively investigated in consideration of its low cost, convenient synthesis and relatively high conductivity [18]. Wang et al. [16a] have synthesized whisker-like PANI which was grown on the surface of OMC. This PANI/OMC composite was used as a positive electrode, showing excellent capacitance (900 F g^{-1}) at a low current density of 0.5 A g^{-1}. The effect of compounding process on electrochemical capacitive properties of PANI/OMC composites has been studied by Li et al. [16b]. The results showed that compared with the physically mixed composite, the *in situ* synthesized PANI/OMC composites exhibited higher specific capacitance at a low current density of 0.1 A g^{-1}. However, the above high specific capacitances of PANI/OMC composites were reported to be obtained in acid medium and in positive potential range since the redox reaction of PANI usually occurs in positive potential range and PANI usually loses its electrochemical activity at pH > 4 [19,20].

Recently, highly ordered mesoporous carbon–silica nanocomposites with interpenetrating networks were synthesized in our group by a triconstituent co-assembly method [21]. After the removal of silica, a great many small pores (including micropores and smaller mesopores) are generated inside the carbon walls. Consequently, the obtained novel ordered mesoporous carbon, named MPC, showed high surface area, large pore volumes and unique multimodal pore structure. Therefore, it provides an ideal substrate to prepare PANI/OMC composites for the electrode materials of supercapacitors.

Herein, we report the syntheses of uniform composites of polyaniline and ordered mesoporous carbon with bicontinuous interpenetrating framework by using this novel ordered mesoporous carbon MPC as the host. The formation of the composites of PANI/MPC was conducted via *in situ* chemical oxidative polymerization of aniline adsorbed in the pores of MPC. The incorporated PANI not only coated a thin layer on the inner surface of the primary mesopores, but also embedded in the small pores inside the carbon walls of MPC to construct bicontinuous interpenetrating framework. These composites provide great advantages as electrode materials in supercapacitors. On one hand, the primary mesochannels of the composites remained large enough for fast electrolyte diffusion; on the other hand, the interpenetrating framework facilitates the contact of the two components for efficient interaction. We have demonstrated for the first time that in a strong alkaline solution, the PANI/MPC composites show excellent redox activities in negative potential range as a result of the strong interaction between the two interpenetrating components. The maximum specific capacitance of the PANI/MPC composites is as high as 400 F g^{-1} at a high current density of 1 A g^{-1} in negative potential range (−0.7 to 0 V *vs.* Hg/HgO) because of the pseudocapacitance generated by the redox reaction. Therefore, it is a good candidate for negative electrode materials in hybrid supercapacitors.

Table 1
Preparation conditions of PANI/MPC and PANI content in PANI/MPC composites.

	Aniline concentration (wt%)	PANI content (wt%)[a]
PANI/MPC-1	4.3	22.3
PANI/MPC-2	8.5	30.2
PANI/MPC-3	16.6	46.6
PANI/MPC-4	39.3	55.5

[a] PANI content was determined from elemental analysis results.

2. Experimental

2.1. Materials synthesis

The novel ordered mesoporous carbon MPC with multimodal pore structure was synthesized on the basis of triconstituent co-assembly approach by using triblock copolymer F127 as a structure-directing agent, soluble phenolic resins and tetraethyl orthosilicate (TEOS) as carbon and silica sources [21]. In a typical process, 1.6 g of block copolymer Pluronic F127 was dissolved in 8.0 g of ethanol containing 1.0 g of (0.2 M) HCl. The mixture was stirred for 1 h at 40 °C to afford a clear solution. Then 2.08 g of TEOS and 5.0 g of (20 wt%) resols' ethanol solution were added to the solution. The mixture was stirred for 2 h and then transferred to dishes. It took 5–8 h at room temperature to evaporate ethanol and 24 h at 100 °C in an oven to thermopolymerize. The as-made flaxen and transparent product was collected and ground into fine powder. Calcination was carried out in a tubular furnace at 900 °C for 2 h under N_2 flow with a heating rate of 1 °C min^{-1} below 600 °C and 5 °C min^{-1} above 600 °C. The ordered mesoporous carbon–silica nanocomposite was immersed in 10 wt% HF solution for 24 h to remove silica. Then MPC with multimodal pore structure was obtained. PANI/MPC composites with different PANI contents were prepared through *in situ* polymerization of aniline initiated by ammonium persulfate (APS) after adsorption of the monomer in the pores of MPC. In a typical preparation, 0.15 g of MPC was added in 30 ml of aniline ethanol solutions of different concentrations (Table 1) with stirring for 24 h at room temperature. The MPC loaded with different amounts of aniline were then immersed in (0.2 M) aqueous solution of HCl containing the same amount (mol) of oxidant initiator APS. Polymerization is continued with continuous stirring at room temperature for 24 h. The suspended powders were filtrated out and washed several times with aqueous HCl solution and ethanol, and vacuum dried at room temperature over night. The obtained composites were denoted as PANI/MPC-1, 2, 3, 4 for the composites containing 22.3, 30.2, 46.6 and 55.5 wt% PANI, respectively. Pure PANI was synthesized under similar conditions. The physical mixture of PANI and MPC was prepared by mixing 0.13 g pure PANI and 0.15 g MPC thoroughly. This physically mixed composite with 46 wt% PANI content was named as PANI/MPC-P.

2.2. Materials characterization

The small-angle X-ray scattering (SAXS) measurements were taken on a Nanostar U small-angle X-ray scattering system (Bruker, Germany) using Cu KR radiation (40 kV, 35 mA). The *d*-spacing values (d) were calculated by the formula $d = 2\pi/q$, and the unit cell parameters (a_0) were calculated from the formula $a_0 = 2d_{10}/\sqrt{3}$. Nitrogen sorption isotherms were measured at 77 K with

a Micromeritics Tristar 3020 analyzer. Before the measurements, the samples were degassed at 150 °C in vacuum for 10 h. The Brunauer–Emmett–Teller (BET) method was utilized to calculate the specific surface areas (S_{BET}) using adsorption data in a relative pressure range from 0.04 to 0.2. Pore size (D) analysis was performed by applying proper nonlocal density functional theory (NLDFT) methods from the adsorption branches of isotherms, and the total pore volumes (V_t) were estimated from the adsorbed amount at a relative pressure P/P_0 of 0.995. The micropore volumes (V_m) and micropore surface areas (S_m) were calculated from the V–t plot method using the equation $V_m/cm^3 = 0.001547\,I$, where I represents the y intercept in the V–t plots. The t values were calculated as a function of the relative pressure using the de Bore equation, $t/Å = [13.99/(\log(P_0/P) + 0.0340)]^{1/2}$. Transmission electron microscopy (TEM) experiments were conducted on a JEOL 2011 microscope operated at 200 kV. Scanning electron microscopy (SEM) images were taken with a Philips XL30 electron microscope operating at 20 kV. A thin gold film was sprayed on the sample before this characterization. Fourier transform infrared (FT-IR) spectra were collected on a Nicolet Fourier spectrophotometer, using KBr pellets of the solid samples. The C, H and N contents were measured on a Vario EL III elemental analyzer (Germany).

2.3. Electrochemical measurement

The electrodes were prepared as follow: the mixture containing 85 wt% active materials, 10 wt% acetylene black, and 5 wt% polytetrafluoroethylene (PTFE) were well mixed, and then pressed onto nickel foam that served as a current collector. The electrochemical experiments were carried out using a three-electrode cell, in which platinum and Hg/HgO electrodes (0.052 V *vs.* the normal hydrogen electrode, NHE) were used as counter and reference electrodes, respectively. The electrolyte was 6 M KOH solution. Cyclic voltammetry and charge–discharge tests were performed using electrochemical analyzer, CHI 606B under ambient condition. The electrochemical impedance spectroscopy (EIS) measurements were performed at −0.3 V *vs.* Hg/HgO using a Solartron Instrument model 1287 electrochemical interface and 1255B frequency response analyze controlled by a computer. Data were collected in the frequency range of 0.1 Hz–1000 kHz.

3. Results and discussion

3.1. Materials characterization and structure analysis

The FT-IR spectra of pure PANI (a), PANI/MPC-1 (b), PANI/MPC-2 (c), PANI/MPC-3 (d), PANI/MPC-4 (e), and MPC (f) are shown in Fig. 1. In the spectrum of pure PANI (a), characteristic bands of PANI appear at 1556 and 1481 cm^{-1} for the stretching vibration of C=C in the quinonoid and benzenoid rings, respectively;

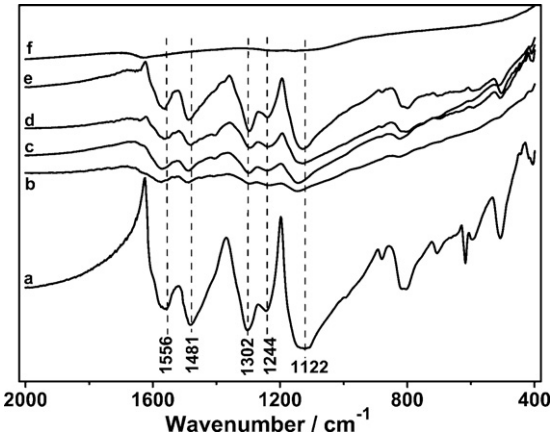

Fig. 1. FT-IR spectra of pure PANI (a), PANI/MPC-1 (b), PANI/MPC-2 (c), PANI/MPC-3 (d), PANI/MPC-4 (e), and MPC (f).

1302 and 1244 cm^{-1} for the stretching vibration of C–N of the secondary aromatic amine and of $CN^{\bullet+}$ in the polaron structure of PANI, respectively; 1122 cm^{-1} for the stretching vibration of C=N in –N=quinoid=N– [22,23]. Upon composite with MPC to form PANI/MPC-1, 2, 3 and 4 containing 22.3, 30.2, 46.6, and 55.5 wt% PANI, respectively, some typical bands shift to higher wavenumbers. The C=C stretching vibration of the quinonoid ring at 1556 cm^{-1} for pure PANI shifts to 1562, 1564, 1572 and 1574 cm^{-1} for PANI/MPC-4, 3, 2, 1 along with lowering PANI content in the composites. The C=N stretching vibration of –N=quinoid=N– at 1122 cm^{-1} shifts to 1128, 1128, 1144 and 1145 cm^{-1} for PANI/MPC-4, 3, 2, 1, respectively. In addition, the intensity ratio of 1556/1481 cm^{-1} increases with the decrease of the PANI content. These results clearly show a strong interaction between PANI and the carbon host. Similar phenomenon has been observed before in the composites of PANI and carbon nanotubes, which was described to be related to a site-selective interaction between the quinonoid ring and carbon [24].

SEM images show that the host MPC exhibits stone-like morphology with irregular shapes (Fig. 2a and b). Composites PANI/MPC-1, PANI/MPC-2 and PANI/MPC-3 with low loading amount of PANI show similar morphologies to their host MPC. Virtually no polymer is observed on particle surfaces of these composites (Fig. 2c–h). It indicates that the polymerization takes place entirely in the pores rather than on the outer surface of MPC [25]. However, when the aniline concentration in the soaking solution increases to 39.3 wt%, the outer surface of the obtained composite PANI/MPC-4 is covered with PANI agglomerates (Fig. 2i and j), suggesting that excess polymers were formed on the outside of the host, which may block the pores to some extent.

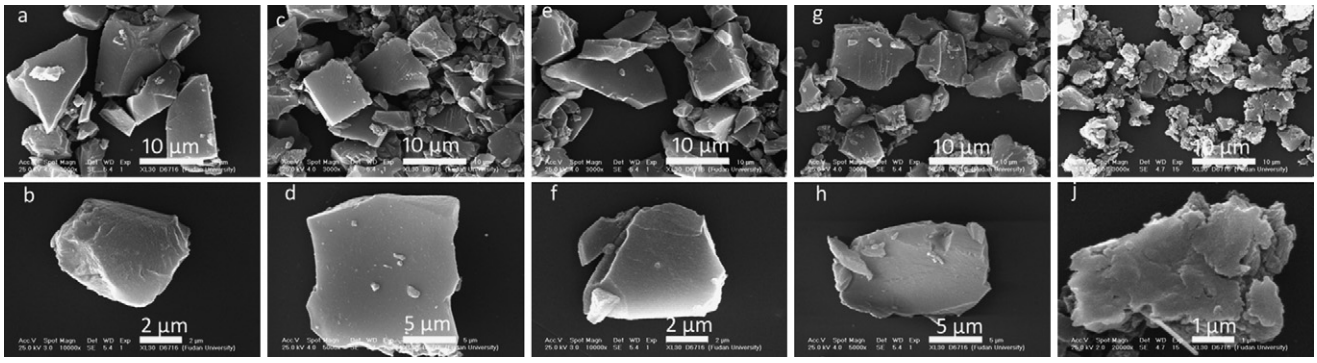

Fig. 2. SEM images of MPC (a and b), PANI/MPC-1 (c and d), PANI/MPC-2 (e and f), PANI/MPC-3 (g and h), and PANI/MPC-4 (i and j).

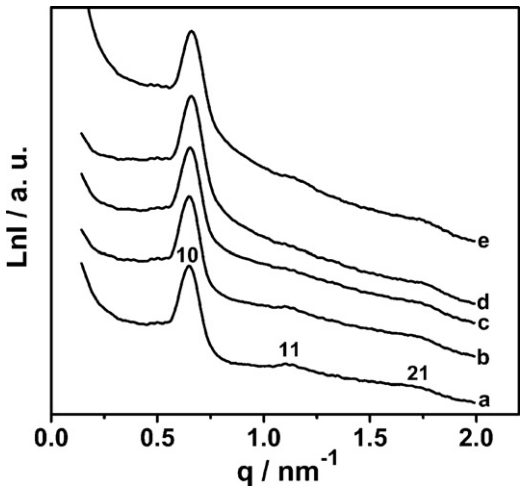

Fig. 3. SAXS patterns of MPC (a), PANI/MPC-1 (b), PANI/MPC-2 (c), PANI/MPC-3 (d), and PANI/MPC-4 (e).

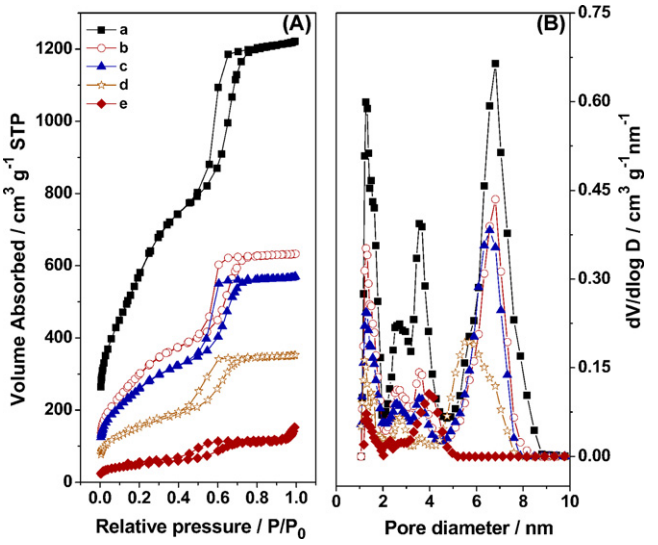

Fig. 5. N_2 sorption isotherms (A) and pore size distributions (B) of MPC (a) and PANI/MPC composites PANI/MPC-1 (b), PANI/MPC-2 (c), PANI/MPC-3 (d), and PANI/MPC-4 (e).

The SAXS patterns of the host MPC and PANI/MPC composites are present in Fig. 3. Three well-resolved scattering peaks are observed for MPC, revealing highly ordered 2-D hexagonal mesostructure (*p6mm*) with unit cell parameter of 11.2 nm. All the PANI/MPC composites exhibit analogous patterns to MPC. One strong diffraction together with two weak and wide peaks is observed. These results clearly indicate that the highly ordered mesostructure is well retained after the incorporation of PANI into the pores. The mesostructure of the host MPC and PANI/MPC composites are further demonstrated by TEM images, as shown in Fig. 4. Similar to MPC, typical stripe-like TEM images viewed from the [1 1 0] direction are observed in all PANI/MPC composites. Remarkably, some whisker-like polymer species are observed at the edge of the mesochannels in the PANI/MPC-4 sample with the highest PANI content (Fig. 4e), which indicates that the polymerization of incorporated aniline also occurred on the outer surface.

N_2 sorption isotherms and pore size distribution curves obtained by using nonlocal density functional theory (NLDFT) method for the host MPC and PANI/MPC composites are shown in Fig. 5A and B, while the physical–chemical properties are summarized in Table 2. MPC exhibits type IV isotherms with distinct capillary condensation steps, which is characteristic of ordered mesoporous materials with narrow pore size distributions. Remarkably, a distinctly increased sorption in the isotherm curves

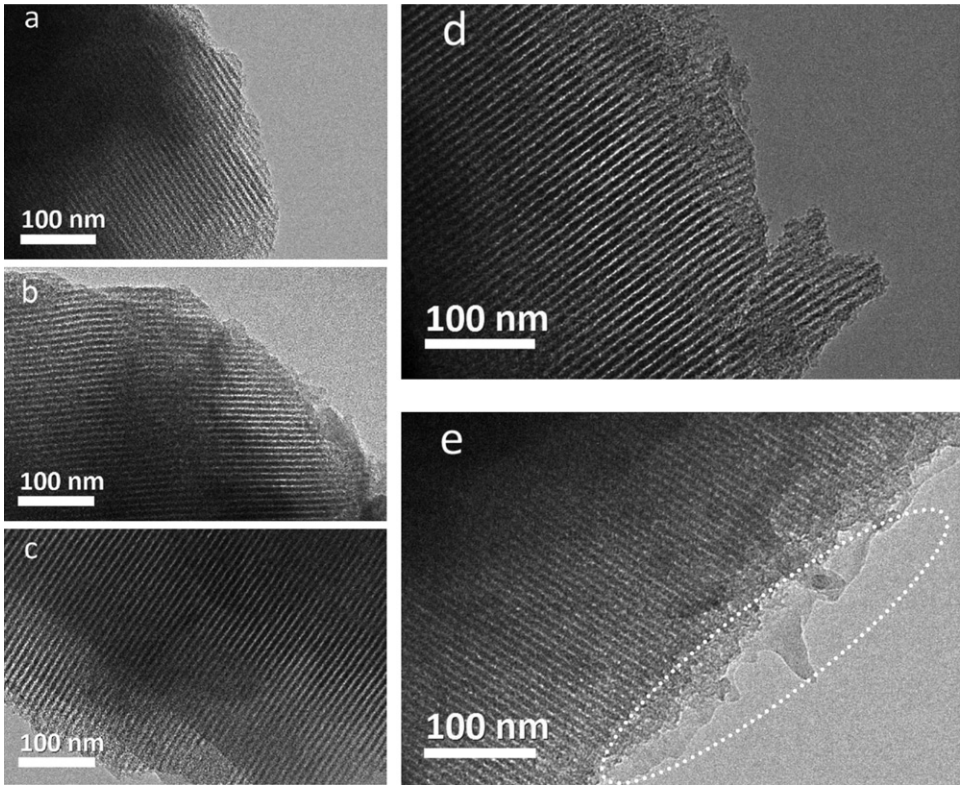

Fig. 4. TEM images of MPC (a), PANI/MPC-1 (b), PANI/MPC-2 (c), PANI/MPC-3 (d), and PANI/MPC-4 (e).

Table 2
Physical–chemical properties of MPC and PANI/MPC composites.

	a_0 (nm)	S_{BET} ($m^2\ g^{-1}$)	S_m ($m^2\ g^{-1}$)	V_t ($cm^3\ g^{-1}$)	V_m ($cm^3\ g^{-1}$)	D_p (nm)
MPC	11.2	2210	1160	1.89	0.55	6.8
PANI/MPC-1	11.2	1120	560	0.98	0.26	6.8
PANI/MPC-2	11.1	960	420	0.88	0.19	6.6
PANI/MPC-3	11.0	560	160	0.54	0.07	5.7
PANI/MPC-4	11.0	180	50	0.24	0.02	4.0

a_0: unit cell parameter; S_{BET}: total BET surface area; S_m: mircopore surface area. V_t: total pore volume; V_m: micropore volume; D_p: primary mesopore diameter.

at relative pressure of P/P_0 of 0.1–0.3 is observed for the MPC (Fig. 5A), corresponding to small pores with a wide distribution below 4.0 nm. The multimodal pore structure of MPC can be more clearly observed from the pore size distribution curve in Fig. 5B. Except for the primary mesopore with a diameter at 6.8 nm, MPC also possesses smaller mesopores centered at 3.6 and 2.7 nm and abundant micropores. These smaller mesopores and most of the micropores inside the carbon walls are caused by the removal of the silica from the carbon–silica composites [21], resulting in high surface area ($2210\ m^2\ g^{-1}$) and large pore volume ($1.89\ cm^3\ g^{-1}$). All PANI/MPC composites show similar type IV isotherms (Fig. 5A). However, the distinct sorption at relative pressure of P/P_0 of 0.1–0.3 in the isotherm curves of the composites gradually disappears with the increase of PANI loading. These results indicate that the small pores inside the carbon walls are gradually filled with PANI upon increasing the loading amount of the polymer in the composites. This is also testified by the pore size distributions in Fig. 5B. For PANI/MPC-1 with the lowest PANI content of 22.3 wt%, the primary mesopore size is the same as that of the host MPC. However, the absorption volume related to the smaller mesopores (Fig. 5B), as well as the micropore surface area (S_m) and micropore volume (V_m) (Table 2) decrease obviously. When PANI contents in the composites further increase, the pore volume for the smaller mesopores together with S_m and V_m further decreases, which indicates more and more polymer has been encapsulated in the small pores inside the carbon walls to form bicontinuous interpenetrating framework. At the same time, the primary mesopore size is found to decrease from 6.6 nm for PANI/MPC-2 to 5.7 nm for PANI/MPC-3 and then to 4.0 nm for PANI/MPC-4, suggested a thin layer of polymer has been coated on the inner surface of the primary mesopores.

Based on the above results, we propose the mesostructure of the PANI/MPC composites as shown in Fig. 6. In the process of aniline adsorption, aniline was preferentially adsorbed in the interpenetrating small pores inside the carbon walls due to stronger capillary force in the smaller pores than in the larger primary mesopores. Then the smaller pores were filled by PANI in the following *in situ* polymerization procedure to form composites with the unique bicontinuous interpenetrating framework. When the aniline concentration in the soaking solution is as low as 4.3 wt%, aniline is almost entirely adsorbed in the small pores. After the *in situ* polymerization, PANI is mainly encapsulated in the small pores inside the carbon walls to afford PANI/MPC-1 with the lowest PANI content (22.3 wt%). Along with the increase in aniline concentration to 8.5 wt%, more aniline can be absorbed not only in the small pores but also in the primary mesochannels. After the following *in situ* polymerization, the polymers can be thereby embedded in the small pores inside the carbon walls and also coat a thin layer on the inner surface of the primary mesochannels to afford PANI/MPC-2 with 30.2 wt% PANI. As the PANI content increases to 46.6 wt% in PANI/MPC-3, nearly all the small pores in the carbon walls are filled with the polymer, only leaving some ultra micropores free as they are too small for the monomer and oxidant initiator to reach. Upon increasing the aniline concentration in the soaking solution to as high as 39.3 wt%, the following *in situ* polymerization could also occur on the outer surface of the host MPC to give PANI/MPC-4 with the highest PANI content (55.5 wt%). However, the polymers on the outer surface could partly block the mesochannels.

3.2. Electrochemical behaviors of PANI/MPC composites

The cyclic voltammogram (CV) of the host MPC in alkaline solution displays rectangular shape (Fig. 7a), which is typical characteristic of double-layer capacitance. The current density on the CV of pure PANI is quite small (Fig. 7b), indicting its poor conductivity in alkaline solution at this negative potential range, which is consistent with the previous report [26]. Interestingly, the CVs of the PANI/MPC composites show a pair of distinct redox peaks between 0.0 and −0.42 V (*vs.* Hg/HgO) (Fig. 7c–f). By contrast, the CV of the physical mixture of PANI and MPC (PANI/MPC-P) shows no redox peak in this potential range (Fig. 7g). It has been reported that compounds built-up with aromatic structure can strongly interact with the basal plane of graphitic surfaces *via* π-stacking [27,28]. Carbon nanotubes can even be dissolved in aniline *via* forming

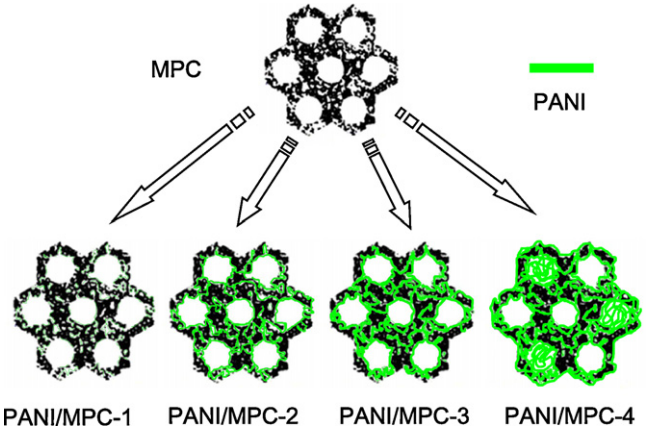

Fig. 6. Schematic illustration for mesostructure of the PANI/MPC composites with different PANI loadings.

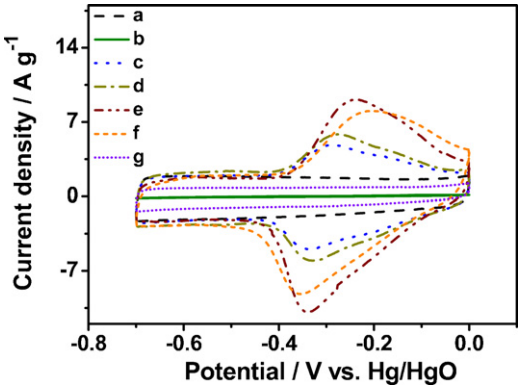

Fig. 7. Cyclic voltammograms of MPC (a), pure PANI (b), PANI/MPC-1 (c), PANI/MPC-2 (d), PANI/MPC-3 (e), PANI/MPC-4 (f), and PANI/MPC-P (g) in 6 M KOH, scan rate: $10\ mV\ s^{-1}$.

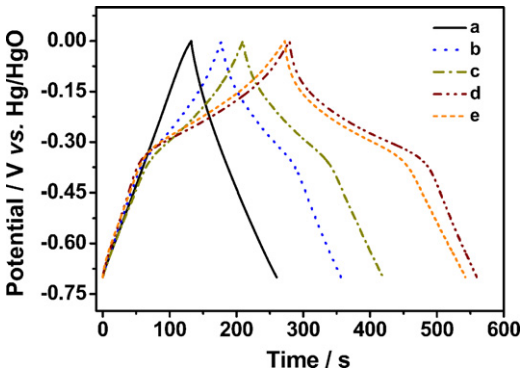

Fig. 8. Charge–discharge curves of MPC (a), PANI/MPC-1 (b), PANI/MPC-2 (c), PANI/MPC-3 (d), and PANI/MPC-4 (e) in 6 M KOH at a current density of 1 A g^{-1}.

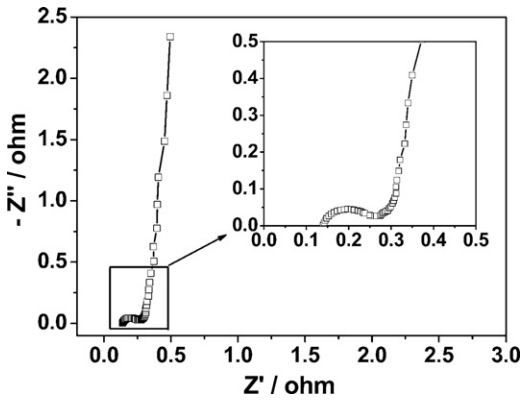

Fig. 9. Nyquist plot for the PANI/MPC-3 composite electrode.

donor–acceptor complex as the former is a good electron acceptor, while the latter is a fairly good electron donor [29]. The carbon nanotubes can act as dopant for PANI [30,31], and the effective site-selective interactions between the π-bonds in the aromatic ring of PANI and the graphitic structure of carbon nanotube facilitate charge-transfer reaction [32]. In our work, the host MPC can act as dopant for PANI through charge-transfer interactions, which does not occur in the physical mixture of PANI and MPC. The interactions can be evidenced by the shifts of vibrational bands in the FT-IR spectra (Fig. 1). The redox pair which appears on the CVs may be related to the electron transfer between the conjugated structure of PANI and π-bonded surface of the host. In addition, as the PANI content in the composites increases from 22.3 to 30.2 wt% and then further to 46.6 wt%, the redox peak current density on the CVs also gradually increases. However, when the PANI content further increases to 55.5 wt% in PANI/MPC-4, the redox peak current density is a bit lower than that of PANI/MPC-3. Besides, compared with those of PANI/MPC-3, the anodic peak potential of PANI/MPC-4 is more positive while the cathodic peak potential is more negative. The reduction in redox peak current density and shift in redox peak potentials may be related to its structure. There are many aggregated PANI observed on the outer surface of PANI/MPC-4 as shown in SEM and TEM images (Figs. 2i and j and 4e). These aggregated PANI on the outer surface fails to contact with the host MPC thoroughly. The interaction between the aggregated PANI and MPC is so weak that it makes few contributions to charge accumulation. Moreover, the aggregated PANI on the outer surface may plug up the pores and block the penetration of electrolyte, which inhibits the contact of active material with the electrolyte. This may increase resistance effect in the PANI/MPC-4 composite electrode and hence increases the difference of anodic and cathodic peak potentials.

The charge–discharge curve of MPC conducted at 1 A g^{-1} in 6 M KOH (Fig. 8a) shows that the response is almost linear and symmetric. While the charge–discharge curves of the PANI/MPC composites show evidently two stages: one is between 0.0 and −0.4 V; the other is between −0.4 and −0.7 V (Fig. 8b–e). At the former, the PANI/MPC composite exhibits longer charge/discharge duration, indicating a great enhanced charge storage capacity, which is attributed to the combination of double-layer capacitance and pseudocapacitance. At the latter stage, the PANI/MPC composite shows shorter charge/discharge duration. This comparatively lower charge storage capacity can be ascribed to the pure double-layer capacitance. These results are in good agreement with the CVs. The specific capacitance of MPC at a current density of 1 A g^{-1} is *ca.* 183 F g^{-1}, while the capacitance of the PANI/MPC composites is much larger due to the additional pseudocapacitance. The specific capacitance of PANI/MPC-1 with 22.3% PANI content is 256 F g^{-1}. Upon increasing PANI content in the composites to obtained PANI/MPC-2 (30.2% PANI) and PANI/MPC-3 (46.6% PANI), the specific capacitance increases to 299 and 400 F g^{-1}, respectively. However, when the PANI content increases to 55.5 wt% in composite PANI/MPC-4, the specific capacitance decreases slightly to 386 F g^{-1}. This variation in specific capacitance of the composites is fairly consistent with the electrochemical activities demonstrated by the CVs, indicating that the redox reaction plays a vital role in the enhancement of the overall specific capacitance.

To evaluate the resistance which is significantly related to power performance, the composite PANI/MPC-3 which shows the highest specific capacitance was investigated by electrochemical impedance spectroscopy (EIS). The Nyquist plot of the PANI/MPC-3 composite electrode is shown in Fig. 9. The semicircle in the high-frequency region is attributed to the charge-transfer resistance of the electrode (R_{ct}) [33]. The high-frequency intercept with the real axis is related to the internal resistance (R_s), which includes the resistance of the electrolyte solution, the intrinsic resistance of the active material and the contact resistance at the interface active material/current collector [34]. R_s is estimated to be about 0.14 Ω. From the diameter of the semicircle on the real axis, R_{ct} is calculated to be 0.11 Ω. The low resistance of the PANI/MPC-3 composite electrode makes it possible for high power performance.

Rate capability of the composite PANI/MPC-3 was investigated by charge–discharge at different current densities. As shown in Fig. 10, the specific capacitance of PANI/MPC-3 composite electrode only decreases 9% when the discharge current density increases from 1 to 20 A g^{-1}. These results demonstrate that the composite PANI/MPC-3 possesses good rate capability, which is necessary for electrode materials of a supercapacitor with high power density.

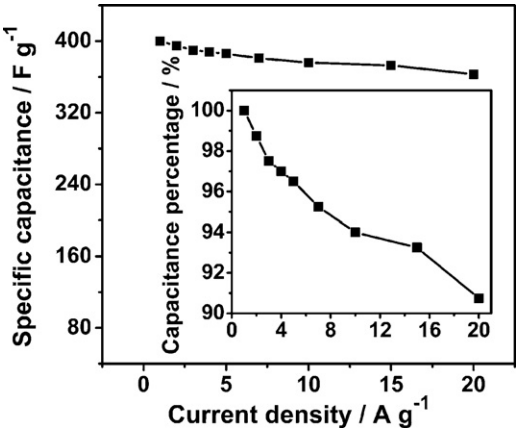

Fig. 10. Specific capacitance of the composite PANI/MPC-3 obtained through charge–discharge at different current densities. The inset is percentage of capacitances obtained at different current densities compared to that obtained at 1 A g^{-1}.

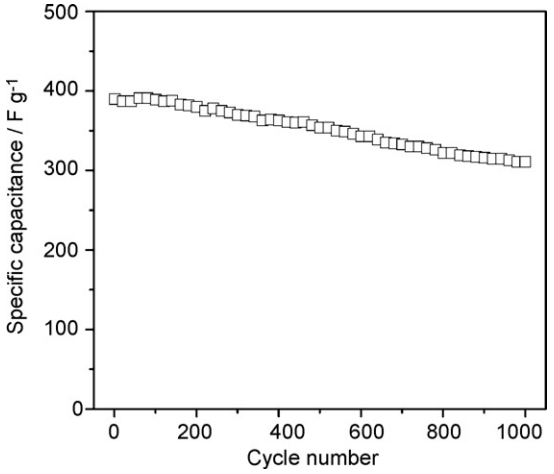

Fig. 11. Variation of specific capacitance with cycle number for the PANI/MPC-3 composite electrode in 6 M KOH at a current density of 3 A g^{-1}.

The good rate performance of PANI/MPC-3 can be attributed to its unique structure. Firstly, the inner surface of the mesochannels in PANI/MPC-3 is covered with PANI which is more hydrophilic. So the mesochannels of PANI/MPC-3 is easily wetted by the aqueous electrolyte. Secondly, as large portion of the incorporated PANI is embedded in the carbon walls of MPC, leaving the primary mesopores large enough (5.7 nm, see Table 2) for the fast penetration of electrolyte. Thirdly, the thickness of uniformly distributed PANI on the inner surfaces of mesopores is just 5–6 Å. Therefore, the diffusion and migration length of the electrolyte ions in PANI during fast charge/discharge process is greatly shortened.

The electrochemical stability of the PANI/MPC-3 composite electrode was examined in 6 M KOH through constant charge–discharge at a current density of 3 A g^{-1} and the data are shown in Fig. 11. The specific capacitance of PANI/MPC-3 is 390 F g^{-1} in the initial cycle. After 1000 consecutive cycles, the specific capacitance gradually decreases to 311 F g^{-1} (*ca.* 80% retention), which is still much higher than most of other reported carbon materials.

4. Conclusion

PANI/MPC composites have been synthesized via *in situ* chemical oxidative polymerization of aniline adsorbed in advance inside the pores of highly ordered mesoporous carbon MPC which possesses interpenetrating small pores inside the carbon walls in addition to large primary mesopores. In all of the PANI/MPC composites with PANI contents from 22.3 to 55.5 wt%, the small pores inside the carbon walls are gradually filled with the incorporated PANI as aniline was preferentially adsorbed in the smaller pores due to the stronger capillary force, resulting in bicontinuous interpenetrating framework for the two components. Along with the increase in PANI content, the *in situ* polymerization also occurred in large primary mesopores but coated a thin layer on the inner surface, so the size of the large primary mesopores was remained more than 4.0 nm. The well ordered mesostructure of the host MPC was maintained in all of the composites as well. A novel redox behavior was discovered for the PANI/MPC composites in a strong alkaline medium in negative potential range due to the interaction between PANI and the host MPC; though other reported PANI samples and PANI based composites are only electrochemical active in acidic solutions and at positive potential range. A maximum specific capacitance of 400 F g^{-1} was obtained for the composites at a high current density of 1 A g^{-1} between −0.7 and 0 V in 6 M KOH. In addition, experiments on the sample that showed the highest specific capacitance indicated that the composite also exhibited good rate capability. The capacitance retention was as high as 91% even if the current density increased from 1 to 20 A g^{-1}. Therefore, the composite provides a new kind of excellent negative electrode materials for hybrid supercapacitors.

Acknowledgements

We sincerely thank Dr. Wangjun Cui for his generous help with EIS investigation. This work was partially supported by National Natural Science Foundation of China (50973013 and 20821140537) and Shanghai Nanotech Promotion Center (0852nm00100).

References

[1] B.E. Conway, Electrochemical Supercapacitors: Scientific Fundamentals and Technological Applications, Kluwer Academic/Plenum Publishers, New York, 1999.
[2] P. Simon, Y. Gogotsi, Nat. Mater. 7 (2008) 845.
[3] Q.T. Qu, P. Zhang, B. Wang, Y.H. Chen, S. Tian, Y.P. Wu, R. Holze, J. Phys. Chem. C 113 (2009) 14020.
[4] V. Khomenko, E. Raymundo-Pinero, F. Beguin, J. Power Sources 153 (2006) 183.
[5] Q.T. Qu, Y. Shi, L.L. Li, W.L. Guo, Y.P. Wu, H.P. Zhang, S.Y. Guan, R. Holze, Electrochem. Commun. 11 (2009) 1325.
[6] C.Z. Yuan, B. Gao, X.G. Zhang, J. Power Sources 173 (2007) 606.
[7] A. Laforgue, P. Simon, J.F. Fauvarque, M. Mastragostino, F. Soavi, J.F. Sarrau, P. Lailler, M. Conte, E. Rossi, S. Saguatti, J. Electrochem. Soc. 150 (2003) A645.
[8] D. Villers, D. Jobin, C. Soucy, D. Cossement, R. Chahine, L. Breau, D. Belanger, J. Electrochem. Soc. 150 (2003) A747.
[9] E. Raymundo-Pinero, F. Leroux, F. Beguin, Adv. Mater. 18 (2006) 1877.
[10] Z.B. Wen, Q.T. Qu, Q. Gao, X.W. Zheng, Z.H. Hu, Y.P. Wu, Y.F. Liu, X.J. Wang, Electrochem. Commun. 11 (2009) 715.
[11] J. Gamby, P.L. Taberna, P. Simon, J.F. Fauvarque, M. Chesneau, J. Power Sources 101 (2001) 109.
[12] H.Y. Liu, K.P. Wang, H.S. Teng, Carbon 43 (2005) 559.
[13] (a) J. Lee, S. Yoon, S.M. Oh, C.H. Shin, T. Hyeon, Adv. Mater. 12 (2000) 359; (b) C. Vix-Guterl, E. Frackowiak, K. Jurewicz, M. Friebe, J. Parmentier, F. Beguin, Carbon 43 (2005) 1293; (c) A.B. Fuertes, F. Pico, J.M. Rojo, J. Power Sources 133 (2004) 329.
[14] (a) H.S. Zhou, S.M. Zhu, M. Hibino, I. Honma, J. Power Sources 122 (2003) 219; (b) W. Xing, S.Z. Qiao, R.G. Ding, F. Li, G.Q. Lu, Z.F. Yan, H.M. Cheng, Carbon 44 (2006) 216.
[15] X.P. Dong, W.H. Shen, J.L. Gu, L.M. Xiong, Y.F. Zhu, H. Li, J.L. Shi, J. Phys. Chem. B 110 (2006) 6015.
[16] (a) Y.G. Wang, H.Q. Li, Y.Y. Xia, Adv. Mater. 18 (2006) 2619; (b) L.X. Li, H.H. Song, Q.C. Zhang, J.Y. Yao, X.H. Chen, J. Power Sources 187 (2009) 268.
[17] J.H. Kim, Y.S. Lee, A.K. Sharma, C.G. Liu, Electrochim. Acta 52 (2006) 1727.
[18] B.K. Kuila, B. Nandan, M. Bohme, A. Janke, M. Stamm, Chem. Commun. (2009) 5749.
[19] H.L. Li, J.X. Wang, Q.X. Chu, Z. Wang, F.B. Zhang, S.C. Wang, J. Power Sources 190 (2009) 578.
[20] A.F. Diaz, J.A. Logan, J. Electroanal. Chem. 111 (1980) 111.
[21] R.L. Liu, Y.F. Shi, Y. Wan, Y. Meng, F.Q. Zhang, D. Gu, Z.X. Chen, B. Tu, D.Y. Zhao, J. Am. Chem. Soc. 128 (2006) 11652.
[22] S. Quillard, G. Louarn, S. Lefrant, A.G. Macdiarmid, Phys. Rev. B 50 (1994) 12496.
[23] S.R. Moraes, D. Huerta-Vilca, A.J. Motheo, Eur. Polym. J. 40 (2004) 2033.
[24] L. Li, Z.Y. Qin, X. Liang, Q.Q. Fan, Y.Q. Lu, W.H. Wu, M.F. Zhu, J. Phys. Chem. C 113 (2009) 5502.
[25] M.S. Cho, H.J. Choi, W.S. Ahn, Langmuir 20 (2004) 202.
[26] W.S. Huang, B.D. Humphrey, A.G. Macdiarmid, J. Chem. Soc. Faraday Trans. I 82 (1986) 2385.
[27] H. Jaegfeldt, T. Kuwana, G. Johansson, J. Am. Chem. Soc. 105 (1983) 1805.
[28] R.J. Chen, Y.G. Zhang, D.W. Wang, H.J. Dai, J. Am. Chem. Soc. 123 (2001) 3838.
[29] Y. Sun, S.R. Wilson, D.I. Schuster, J. Am. Chem. Soc. 123 (2001) 5348.
[30] H. Zengin, W.S. Zhou, J.Y. Jin, R. Czerw, D.W. Smith, L. Echegoyen, D.L. Carroll, S.H. Foulger, J. Ballato, Adv. Mater. 14 (2002) 1480.
[31] H.J. Zhou, Y.Q. Lin, P. Yu, L. Su, L.Q. Mao, Electrochem. Commun. 11 (2009) 965.
[32] M. Cochet, W.K. Maser, A.M. Benito, M.A. Callejas, M.T. Martinez, J.M. Benoit, J. Schreiber, O. Chauvet, Chem. Commun. (2001) 1450.
[33] F. Xu, G.D. Zheng, D.C. Wu, Y.R. Liang, Z.H. Li, R.W. Fu, Phys. Chem. Chem. Phys. 12 (2010) 3270.
[34] S.R. Sivakkumar, W.J. Kim, J.A. Choi, D.R. MacFarlane, M. Forsyth, D.W. Kim, J. Power Sources 171 (2007) 1062.